Numerical analysis of Io's atmosphere based on a model Boltzmann equation : Unsteady behavior during eclipse (Mathematical Analysis in Fluid and Gas Dynamics)

AUTHOR(S):

Kosuge, Shingo

数理解析研究所講究録
第1883巻 2014年 100-112

Numerical analysis of Io's atmosphere based on a model Boltzmann equation: Unsteady behavior during eclipse

Shingo Kosuge
Department of Mechanical Engineering and Science, Kyoto University

1 Introduction

Io is a satellite of Jupiter. The observations made by NASA's spacecrafts in the 1970s (Pioneer and Voyager probes) revealed the existence of volcanic activities and a thin atmosphere mainly composed of sulfur dioxide (SO_2) gas. The surface temperature of Io is considered to vary according to the sunlight between about 90 K and 130 K (except near volcanos). The phase transition of SO_2 occurs in this temperature range: the SO_2 gas condenses to form a (very thin) layer of frost on the ground during the night and, as a result, the atmosphere may almost vanish; conversely, the frost sublimates and the atmosphere is restored during the daytime. The dynamics of Io's atmosphere under sublimation and condensation of SO_2 has been studied for a long time (see, e.g., Refs. [1, 2, 3, 4] and references therein).

The above-mentioned process of atmospheric collapse and reformation is expected to take place also during and after eclipse, during which Io is in the shadow of Jupiter. Moore et. al. [5] tackled such a problem for the first time: they carried out a numerical analysis of the Boltzmann equation by the direct simulation Monte Carlo (DSMC) method [6, 7] to investigate the unsteady one-dimensional behavior of the atmosphere in eclipse. In Ref. [5], the atmosphere was treated as a binary mixture of SO_2 and another minor component (SO or O_2), the latter of which is (partially) noncondensable. The results in Ref. [5] reveal the effect of the noncondensable gas: a trace of noncondensable gas carried by the condensing flow of SO_2 accumulates on the surface at the early stage of eclipse and then acts as a barrier to further condensation to delay the atmospheric collapse significantly. In the meantime, little information on the time evolution and structure of the flow field is available from Ref. [5], mainly because of the stochastic noise inherent in the DSMC results.

In this report, we introduce our recent results in Refs. [8, 9], where essentially the same problem as in Ref. [5] was studied through a different approach after making some

simplifications. First we adopted the model Boltzmann equation proposed in Ref. [10], instead of the full Boltzmann equation, for computational convenience. Second we focused on the effect of the noncondensable gas only, because it was expected to be dominant; we omitted all other effects taken into account in the previous DSMC analysis [5], such as the effect of plasma impingement from the outer space, that of molecular internal structure, and so on. Then we could perform an accurate deterministic computation by means of a finite-difference method at a reasonable computational cost. In spite of those simplifications, however, the overall behavior (the column density of SO_2) during eclipse obtained in our study is quite similar to the previous result [5]. Moreover, as will be seen later in Sec. 5, our solutions with higher temporal and spatial resolution reveal some new phenomena (waves in the profiles of macroscopic quantities and an oscillatory motion), which were not explored in Ref. [5].

2 Problem and assumptions

Consider an atmospheric column over a fixed point on Io's surface near the equator belonging to the sub-Jovian hemisphere.[1] The ground is located at $X_1 = 0$ and is covered by the frost of SO_2, where $\boldsymbol{X}$ $[= (X_1, X_2, X_3)]$ be the space rectangular coordinates.[2] The atmosphere extends over the half-space $X_1 > 0$ and is composed of SO_2 vapor and another noncondensable gas, SO or O_2.[3] The eclipse starts at time $t = 0$ and lasts until $t = 120$ min. The initial atmosphere is assumed to be in a saturated equilibrium state at rest with uniform temperature T_0. The surface temperature T_w, which coincides with T_0 at $t = 0$, varies with time according to the change of insolation [see Eq. (11) below] and then condensation or sublimation of SO_2 may occur. We investigate unsteady behavior of the atmospheric column during eclipse under the following assumptions: (i) the behavior of the atmosphere is described by the model Boltzmann equation for mixtures proposed in Ref. [10]; (ii) the vapor (SO_2 gas) obeys the complete-condensation boundary condition on the surface [see Eq. (7) below]; (iii) the noncondensable gas (SO or O_2) obeys the diffuse-reflection boundary condition on the surface; (iv) the surface and the atmosphere are horizontally uniform [in the length scale of the pressure scale height H ($\sim 7 - 9$ km) of the atmosphere], so that the problem can be treated as a spatially 1-D problem depending on X_1 only.

[1] As a result of tidal locking, Io always shows the same side (the sub-Jovian hemisphere) to Jupiter, so that the eclipse does not much effect the anti-Jovian hemisphere.

[2] The curvature of the surface is ignorable in the present problem.

[3] In reality, SO has not been established as a perfectly noncondensable gas in Io's circumstances.

3 Formulation

In the following, the vapor (SO_2 gas) and noncondensable gas (SO or O_2) will be referred to as species A and B, respectively. The Greek letters α and β will be used to represent the species, i.e., $\alpha, \beta = \{A, B\}$.

Let us denote the velocity distribution function (VDF) of molecules of species α as $F^\alpha = F^\alpha(t, X_1, \boldsymbol{\xi})$, where $\boldsymbol{\xi}$ $[= (\xi_1, \xi_2, \xi_3)]$ is the molecular velocity. The macroscopic quantities, such as the number density n^α, flow velocity $\boldsymbol{v}^\alpha$ $[= (v_1^\alpha, v_2^\alpha, v_3^\alpha)]$, pressure p^α, and temperature T^α of species α, are defined as the moments of F^α as follows:

$$\begin{aligned} n^\alpha &= \int F^\alpha \mathrm{d}\boldsymbol{\xi}, \qquad \boldsymbol{v}^\alpha = \frac{1}{n^\alpha} \int \boldsymbol{\xi} F^\alpha \mathrm{d}\boldsymbol{\xi}, \\ p^\alpha &= k n^\alpha T^\alpha = \frac{1}{3} \int m^\alpha |\boldsymbol{\xi} - \boldsymbol{v}^\alpha|^2 F^\alpha \mathrm{d}\boldsymbol{\xi}, \end{aligned} \tag{1}$$

where m^α is the molecular mass of species α, k is the Boltzmann constant, and $\mathrm{d}\boldsymbol{\xi} = \mathrm{d}\xi_1 \mathrm{d}\xi_2 \mathrm{d}\xi_3$. The domain of integration is the whole space of $\boldsymbol{\xi}$. The corresponding quantities of the total mixture, i.e., the number density n, flow velocity $\boldsymbol{v}$ $[= (v_1, v_2, v_3)]$, pressure p, and temperature T of the mixture, are given by

$$\begin{aligned} n &= \sum_{\alpha=A,B} n^\alpha, \qquad \boldsymbol{v} = \sum_{\alpha=A,B} m^\alpha n^\alpha \boldsymbol{v}^\alpha \Big/ \sum_{\alpha=A,B} m^\alpha n^\alpha, \\ p &= knT = \sum_{\alpha=A,B} \left(p^\alpha + \frac{1}{3} m^\alpha n^\alpha |\boldsymbol{v}^\alpha - \boldsymbol{v}|^2\right). \end{aligned} \tag{2}$$

Note that the horizontal components of the flow velocity will be ignored (i.e., $v_2^\alpha = v_3^\alpha = v_2 = v_3 = 0$) in the actual analysis, whereas they are left in the formulation.

3.1 Model Boltzmann equation

The model Boltzmann equation in Ref. [10] for the present problem may be written as follows:

$$\frac{\partial F^\alpha}{\partial t} + \xi_1 \frac{\partial F^\alpha}{\partial X_1} - g \frac{\partial F^\alpha}{\partial \xi_1} = K^\alpha (M^\alpha - F^\alpha), \quad (\alpha = A, B). \tag{3}$$

Here, g $(= 1.8\ \mathrm{m/s^2})$ is the gravitational acceleration on Io, which is treated as a constant since the scale height H is much smaller than Io's radius R (=1820 km). For the same reason, the effect of planetary rotation (the Coriolis and centrifugal force) is omitted. The K^α and M^α are defined by

$$\begin{aligned} K^\alpha &= \sum_{\beta=A,B} K^{\beta\alpha} n^\beta, \\ M^\alpha &= n^\alpha \left(\frac{m^\alpha}{2\pi k T^{(\alpha)}}\right)^{3/2} \exp\left(-\frac{m^\alpha |\boldsymbol{\xi} - \boldsymbol{v}^{(\alpha)}|^2}{2kT^{(\alpha)}}\right). \end{aligned} \tag{4}$$

The $K^{\beta\alpha}$ $(= K^{\alpha\beta})$ is a positive constant, that determines the collision frequency of an α-species molecule with β-species molecules via $K^{\beta\alpha}n^{\beta}$. Thus, the above K^{α} corresponds to the total collision frequency of an α molecule. The velocity $\boldsymbol{v}^{(\alpha)}$ and temperature $T^{(\alpha)}$ of the Maxwellian M^{α} are defined by

$$\boldsymbol{v}^{(\alpha)} = \boldsymbol{v}^{\alpha} + \frac{2}{m^{\alpha}K^{\alpha}} \sum_{\beta=A,B} \mu^{\beta\alpha}\Omega^{\beta\alpha}n^{\beta}(\boldsymbol{v}^{\beta} - \boldsymbol{v}^{\alpha}), \tag{5a}$$

$$T^{(\alpha)} = T^{\alpha} - \frac{m^{\alpha}}{3k}|\boldsymbol{v}^{(\alpha)} - \boldsymbol{v}^{\alpha}|^2 + \frac{4}{K^{\alpha}} \sum_{\beta=A,B} \frac{\mu^{\beta\alpha}\Omega^{\beta\alpha}n^{\beta}}{m^{\beta}+m^{\alpha}}\Big(T^{\beta} - T^{\alpha} + \frac{m^{\beta}}{3k}|\boldsymbol{v}^{\beta} - \boldsymbol{v}^{\alpha}|^2\Big), \tag{5b}$$

where $\mu^{\beta\alpha}$ $[= m^{\beta}m^{\alpha}/(m^{\beta}+m^{\alpha})]$ is the reduced mass and $\Omega^{\beta\alpha}$ $(= \Omega^{\alpha\beta})$ is an additional positive constant; the positivity of $T^{(\alpha)}$ follows if $\Omega^{\beta\alpha} \leq K^{\beta\alpha}$. Note that Eq. (1) is necessary to complete the model equation because n^{α}, $\boldsymbol{v}^{\alpha}$, and T^{α} appear in Eqs. (4) and (5).

This model was designed in such a way that, by adjusting $\Omega^{\beta\alpha}$, the momentum and energy exchanges between different species can be the same as those for (pseudo-)Maxwell molecules with an arbitrary value of the angular cutoff parameter (see, e.g., Ref. [11]). In the present study, however, this property is not used for specifying the value of $\Omega^{\beta\alpha}$. We first specify K^{AA} by the relation

$$K^{AA} = 4d^2(\pi k T_0/m^A)^{1/2}, \tag{6}$$

where d $(= 7.16 \times 10^{-10}$ m) is the nominal diameter of an SO_2 molecule. This relation means that the molecular mean free path with respect to SO_2–SO_2 collisions in an equilibrium state with temperature T_0 for the model equation is equal to that for the hard-sphere gas with molecular diameter d. Then, for simplicity, K^{BB}, K^{BA}, and Ω^{BA} are all assumed to be identical with K^{AA} [note that Ω^{AA} and Ω^{BB} are unnecessary; see Eq. (5)]. Therefore, pseudo-Maxwell behavior of the molecules is not enforced in the present study.

3.2 Initial and boundary conditions

The boundary condition on the surface is written as follows. For $X_1 = 0$ and $\xi_1 > 0$,

$$F^{\alpha} = n_w^{\alpha}\Big(\frac{m^{\alpha}}{2\pi k T_w}\Big)^{3/2} \exp\Big(-\frac{m^{\alpha}|\boldsymbol{\xi}|^2}{2kT_w}\Big), \tag{7a}$$

$$n_w^A = p_w^A/kT_w, \quad n_w^B = -\Big(\frac{2\pi m^B}{kT_w}\Big)^{1/2} \int_{\xi_1<0} \xi_1 F^B \mathrm{d}\boldsymbol{\xi}. \tag{7b}$$

Here p_w^A is the saturated vapor pressure of SO_2 at temperature T_w and is given by the Clausius–Clapeyron relation:

$$p_w^A = \Pi \exp(-\Gamma/T_w), \quad (\Pi = 1.516 \times 10^{13} \text{ Pa and } \Gamma = 4510 \text{ K}). \tag{8}$$

In the present problem, the variation of T_w and corresponding p_w^A with time would induce the unsteady motion of the atmosphere through the boundary condition (7).

The initial condition is written as follows. At $t = 0$,

$$F^\alpha = n_0^\alpha \Big(\frac{m^\alpha}{2\pi k T_0}\Big)^{3/2} \exp\Big(-\frac{m^\alpha(|\boldsymbol{\xi}|^2 + 2gX_1)}{2kT_0}\Big). \tag{9}$$

Here n_0^α is the initial number density of species α on the surface ($X_1 = 0$); $n_0^A = p_0^A/kT_0$ with p_0^A being the saturated vapor pressure at temperature T_0 [i.e., p_0^A is given by Eq. (8) with T_w being replaced by T_0]. The initial temperature T_0 will be chosen in the next section. The concentration χ^B of the noncondensable gas in the initial atmospheric column is written as

$$\chi^B = \int_0^\infty n^B(t=0)\mathrm{d}X_1 \Big/ \int_0^\infty n(t=0)\mathrm{d}X_1 = \frac{(n_0^B/m^B)}{(n_0^A/m^A) + (n_0^B/m^B)}. \tag{10}$$

In the following, the amount of the noncondensable gas will be specified by χ^B, instead of n_0^B.

3.3 Surface temperature

The surface temperature T_w is determined by the same differential equation as that in Ref. [5]:

$$\frac{\mathrm{d}T_w}{\mathrm{d}t} = \begin{cases} A\sigma(T_{\text{Min}}^4 - T_w^4), & \text{for } 0 \le t \le 120 \text{ min}, \\ A\sigma(T_{\text{E}}^4 - T_w^4), & \text{for } t > 120 \text{ min}, \end{cases} \tag{11}$$

where σ is the Stefan–Boltzmann constant and $A = \varepsilon/C$ with ε being the bolometric emissivity and C the heat capacity per unit area of the surface. The T_{E} is an equilibrium temperature defined as

$$T_{\text{E}} = \begin{cases} (T_{\text{Max}} - T_{\text{Min}})\cos^{1/4}\theta + T_{\text{Min}}, & \text{for } \theta \le 90°, \\ T_{\text{Min}}, & \text{for } \theta > 90°, \end{cases} \tag{12}$$

where θ is the solar zenith angle (SZA), which varies with time according to the diurnal motion of the sun. The maximum and minimum of T_{E} are fixed as $T_{\text{Max}} = 120$ K and $T_{\text{Min}} = 90$ K throughout the following analysis.

TABLE 1: Simulation cases.

Case	T_0 (K)	Longitude (°)	Gas B (χ^B)	A^{-1}(J/m^{2}K)
1	110	69	— (0)	350
2	110	69	SO (0.35)	350
3	110	69	SO (0.35)	700
4	110	69	SO (0.35)	175
5	110	69	O_2 (0.35)	350
6	110	69	O_2 (0.07)	350
7	115	52	— (0)	350
8	115	52	SO (0.22)	350
9	120	351	— (0)	350
10	120	351	SO (0.03)	350

The initial temperature T_0 appearing in Eq. (9) is chosen as $T_0 = T_{\rm E}(t = 0)$ using Eq. (12), after we specify the location of the atmospheric column (i.e., the longitude and latitude) and calculate the SZA θ as a function of time t (note that $t = 0$ is defined to be the time when eclipse starts). It should be noted that the above T_w is influenced only by the insolation and not by the atmospheric behavior (i.e., not by the latent heat and sensible heat from the gas), since the former is dominant. We solve Eq. (11) with the initial condition $T_w(t = 0) = T_0$ to obtain $T_w(t)$ beforehand.

4 Numerical analysis

We first eliminate the molecular-velocity variables ξ_2 and ξ_3 from the initial-boundary value problem (3), (7), and (9) by introducing appropriate marginal VDF's. Then, the reduced problem with three independent variables t, X_1, and ξ_1 is solved by a finite-difference method. We used (i) an implicit scheme in Ref. [12] where the derivatives with respect to X_1 and ξ_1 are expressed by a 2nd-order up-wind finite-difference (see, e.g., Ref. [13]) and (ii) 2nd-order Runge–Kutta (Heun's) scheme along the characteristics of Eq. (3) in combination with the interpolation method devised in Ref. [14]. In the latter scheme, because of the properties of the method in Ref. [14], the transient waves tend to be more accurately captured without overshoots in the profiles of the macroscopic quantities (and in those of the VDF's). However, as in the cubic interpolated pseudo-particle (CIP) method [15], equations for the derivatives of F^α must be solved simultaneously. Thus the latter requires larger amount of computations (and involves some difficulty in the treatment of boundary conditions for the derivatives). To compensate the increased amount of computations, we performed a parallel computing (the latter is an explicit

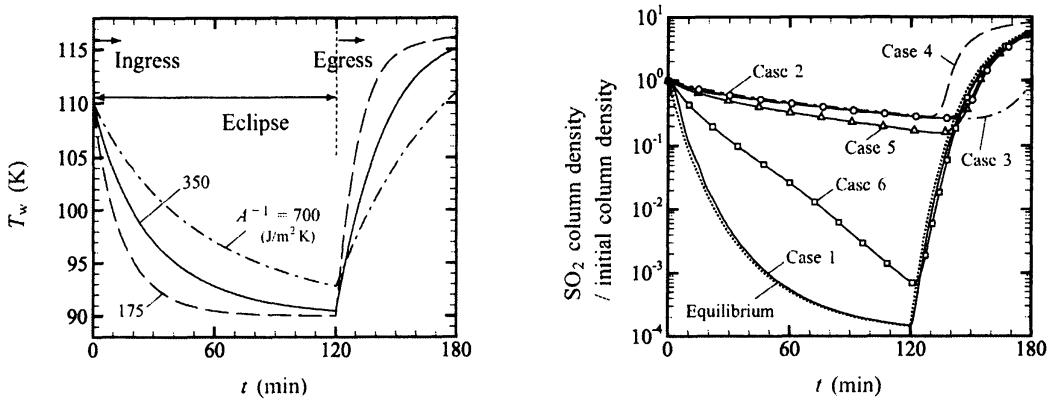

FIGURE 1: Surface Temperature T_w and SO_2 column density vs. time in the case of $T_0 = 110$ K. The initial SO_2 column density is 1.2386×10^{20} #/m^2. The dotted line in the right panel indicates the theoretical value for pure SO_2 atmosphere in an isothermal saturated equilibrium state at rest when $A^{-1} = 350$ J/m^{2}K.

scheme).

The results shown in the next section were obtained by scheme (ii), while the details of the method are omitted here [some test runs with scheme (i) were also performed and gave roughly the same results]. In the computation, we limit the range of X_1 up to $X_1 \sim 282 - 313$ km and impose the specular-reflection condition at the upper boundary[4]; the minimum grid intervals for $T_0 = 110$, 115, and 120 K are, respectively, 15.9 m, 8.3 m, and 4.3 m at $X_1 = 0$; the maximum intervals are about 0.3 – 1.1 km at the upper boundary. The range of ξ_1 is limited as $|\xi_1| \leq 8c_0$, where c_0 [$= (2kT_0/m^A)^{1/2}$] is about 173 m/s for $T_0 = 115$ K; the minimum and maximum grid intervals are $0.005c_0$ at $\xi_1 = 0$ and $0.045c_0$ at $\xi_1 = \pm 8c_0$, respectively. The time steps are about 4.7 ms for $T_0 = 110$ and 115 K and 2.3 ms for 120 K.

5 Results

We consider Cases 1 – 10 listed in Table 1; for simplicity, the column located in the equator (or latitude 0°) is considered in all the cases. The values of parameters in Table 1 were cited from Ref. [5].

Figure 1 shows the variations of the surface temperature and of the column density of SO_2 in the case of $T_0 = 110$ K. The column density of pure SO_2 atmosphere (Case 1) decreases significantly at the end of eclipse, whereas in the case of mixtures the decrease

[4]This condition was used to fix the total amount of the noncondensable gas in the column. A vacuum condition for the vapor, i.e., $F^A(\xi_1 < 0) = 0$ at the upper boundary, was also used in some test runs and gave essentially the same results.

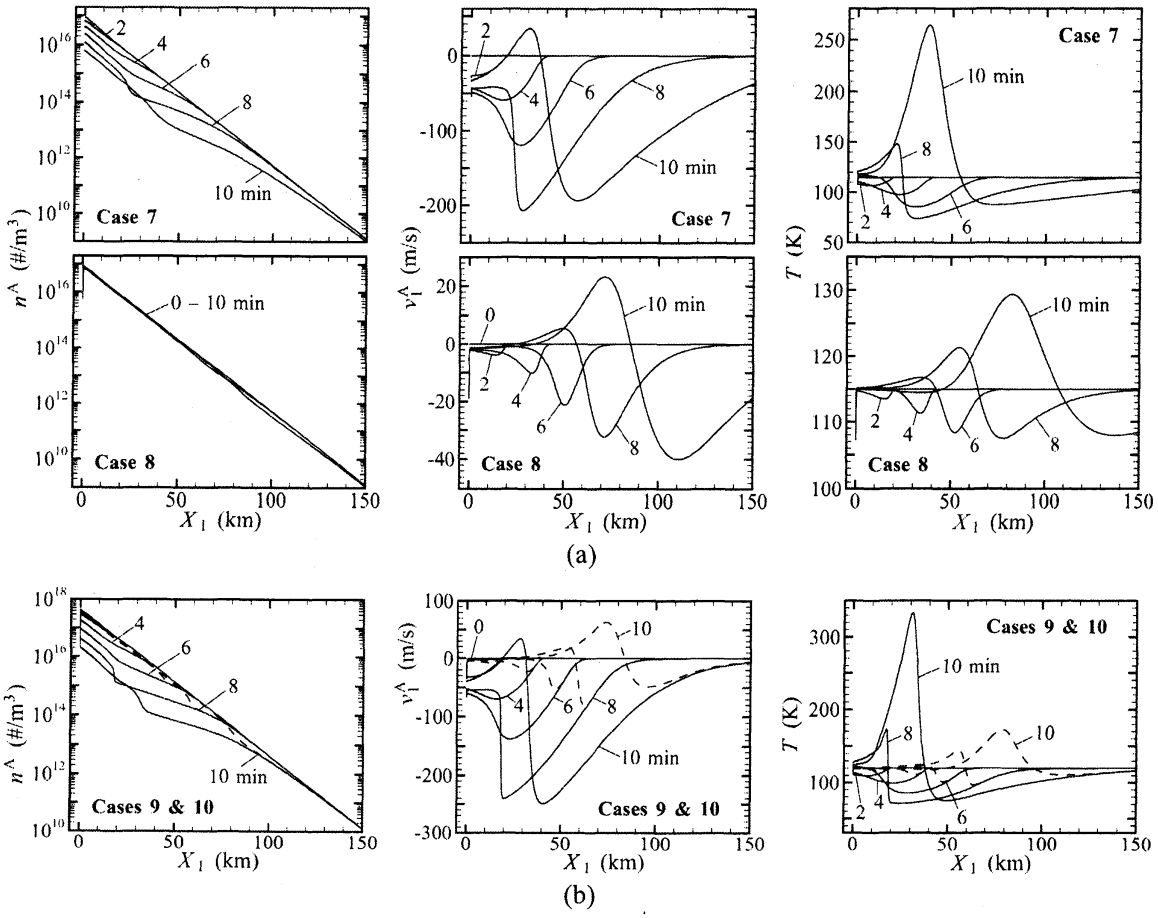

FIGURE 2: Profiles of the macroscopic quantities at every 2 minutes during the first 10 minutes after ingress. (a) Cases 7 and 8, and (b) Cases 9 (solid line) and 10 (dashed line). In (b), each of the dashed lines approaches the corresponding solid line for the same t as $X_1 \to \infty$.

is hindered by the noncondensable gas [see Fig. 3(b) below]. The effects of the gas species (i.e., the molecular mass ratio m^B/m^A), concentration χ^B, and heat capacity of the surface ($\sim A^{-1}$) are also examined. Except for some minor differences, the overall behavior of the column shown in Fig. 1 seems to be close to the corresponding result of the previous DSMC analysis (i.e., Fig. 8 in Ref. [5]).

5.1 During eclipse

Figure 2 shows the profiles of macroscopic quantities at the beginning of eclipse. In Cases 7 and 9 (pure SO_2), a fast condensing flow is induced, and, as a result, an expansion wave is sent upward. The expansion wave is then followed by a shock wave appearing near

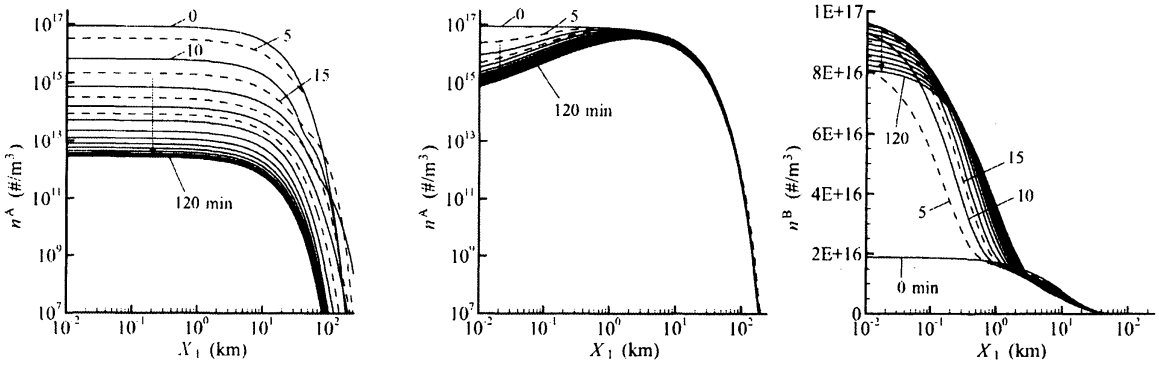

FIGURE 3: Number density profiles during eclipse. (a) Case 7 and (b) Case 8. The solid line indicates profiles at every 10 minutes ($t = 0, 10, \ldots, 120$ min), and the dashed line those at $t = 5$, 15, 25, and 35 min in (a) and those at $t = 5$ and 15 min in (b).

the surface. While propagating upward, the shock wave stretches rapidly because the background pressure decays exponentially with altitude (thus the local mean free path grows exponentially). In Cases 8 and 10 (mixture), the condensing flow is relatively slow because of the hindrance by the noncondensable gas [see Fig. 3(b) below]. The expansion wave is sent as in the pure SO_2 case, but is immediately followed by a relatively weak compression wave.

Figure 3 shows the profiles of the number density in Cases 7 and 8 during eclipse. In Case 7 (pure SO_2), the number density decreases at all altitudes until the end of eclipse except at $t \sim 10 - 30$ min. During that time period, the number density at high altitudes ($X_1 \gtrsim 100$ km) is increased temporarily by the passage of the shock wave seen in Fig. 2. In Case 8 (mixture), the number density of SO_2 decreases only in the neighborhood of the surface and hardly changes at high altitudes. This is because the noncondensable gas, which is carried by the condensing flow of SO_2 to the surface and accumulates there, forms the partial barrier to the atmospheric collapse. The number density of the noncondensable gas near the surface increases rapidly until $t \sim 20$ min and then starts to decrease because of the upward self diffusion.

Figures 4 and 5 show, respectively, the profiles of the flow velocity and temperature in Cases 7 and 8 during eclipse. The oscillatory behavior seen in the figures is produced by waves which, as those in Fig. 2, appear in the lower atmosphere and propagate upward successively. In Case 7, the amplitude of oscillation is large and thus a very fast flow and high temperature may appear instantaneously, especially at high altitudes. The oscillation decays rapidly with time and almost ceases until $t \sim 40$ min. In Case 8, while the amplitude is small compared to the pure SO_2 case and decays with time, the oscillation

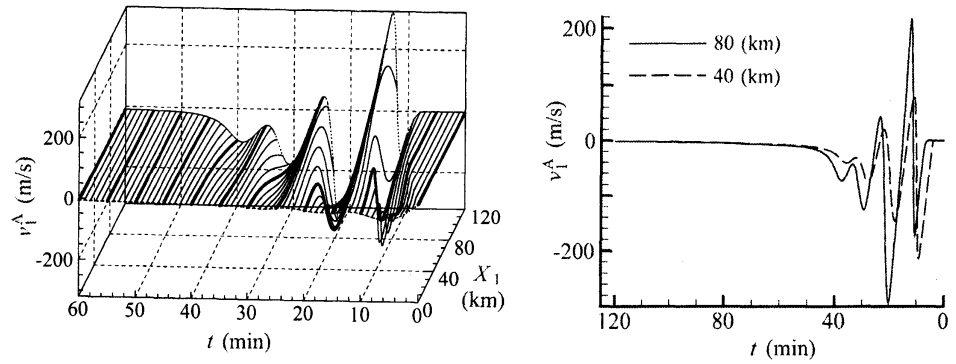

(a) Case 7

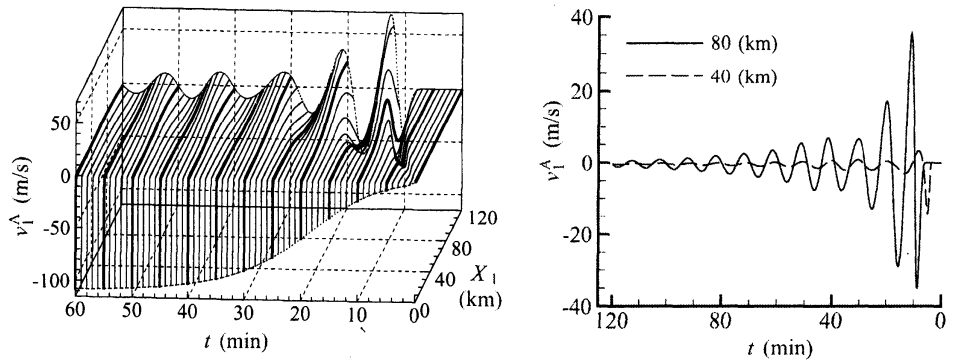

(b) Case 8

FIGURE 4: Profiles of the flow velocity v_1^A at every minute (left panel) and the cross sections at $X_1 \simeq 40$ and 80 km (right panel). (a) Case 7 and (b) Case 8. The thick line in the left panel indicates profiles at every 5 minutes.

continues until the end of eclipse except near the surface. The oscillation period measured from the right panels of Figs. 4(b) and 5(b) is about 10 min, whereas the Brunt–Väisälä period for the initial isothermal atmosphere computed by a textbook formula is about 11.5 min. In Case 8, a fast condensing flow in the close vicinity of the surface remains until the end of eclipse. This is because the SO_2 density on the surface is kept much higher than the saturation density by the effect of the noncondensable gas [see Fig. 3(b)]. The temperature in Case 8 oscillates around the initial temperature ($T_0 = 115$ K) in most parts of the atmosphere. The atmosphere is cooled only near the surface via conduction.

5.2 After egress

Figure 6 shows the profiles of the number density in Cases 7 and 8 after egress. In Case 7, the number density starts to increase immediately after egress and the initial density

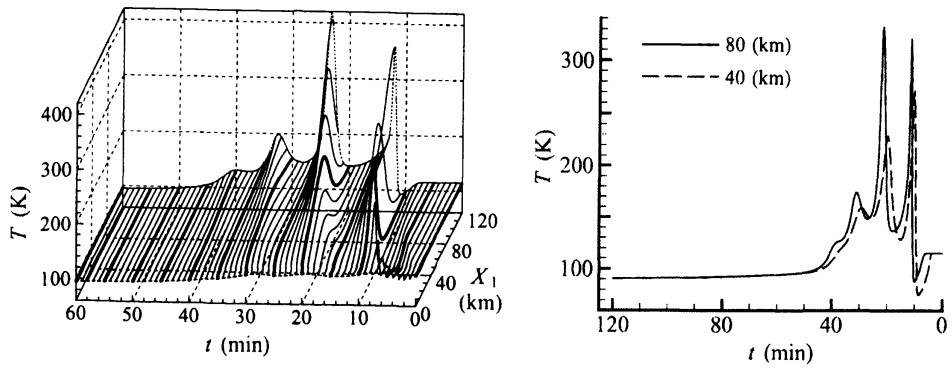

(a) Case 7

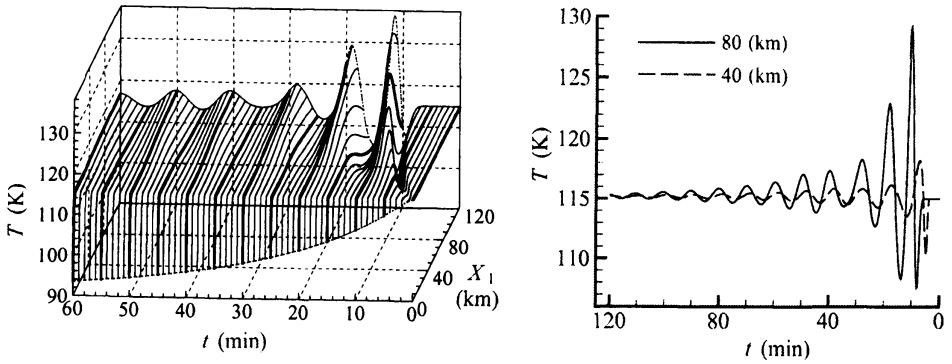

(b) Case 8

FIGURE 5: Profiles of the temperature T at every minute (left panel) and the cross sections at $X_1 \simeq 40$ and 80 km (right panel). (a) Case 7 and (b) Case 8. The thick line in the left panel indicates profiles at every 5 minutes.

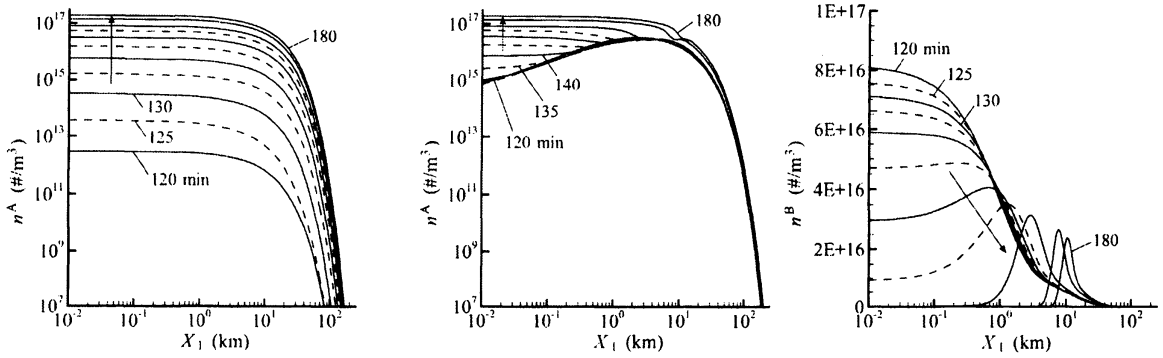

FIGURE 6: Number density profiles after egress. (a) Case 7 and (b) Case 8. The solid line indicates profiles at every 10 minutes ($t = 120, 130, \ldots, 180$ min), and the dashed line those at $t = 125$, 135, 145, and 155 min.

on the surface is restored at $t \sim 160$ min. In Case 8, the number density of SO_2 remains almost unchanged during the first 10 minutes after egress until the surface temperature and the corresponding saturation density increase sufficiently and the sublimation starts. The noncondensable gas is swept upward by the sublimating flow of SO_2 and forms a layer centered around $X_1 = 10$ km at $t = 180$ min. Correspondingly, a hollow is seen in the profile of SO_2 density.

6 Concluding remarks

The unsteady one-dimensional behavior of Io's atmosphere during and after eclipse caused by sublimation and condensation of SO_2 is studied via a numerical analysis of the model Boltzmann equation by means of a finite-difference method. To concentrate on the key physics in this problem, we took into account the effect of the noncondensable gas (SO or O_2) only and ignored other effects included in the previous DSMC analysis [5] (e.g., the plasma impingement, molecular internal structure, and so on). In spite of the simplifications, the column density of SO_2 in eclipse is quite similar to the previous DSMC result. Thus, we may say that the atmospheric collapse and the interruption by a noncondensable gas are, as a whole, correctly reproduced in the present simulation.

The solutions obtained in the present approach may have some restrictions because of the simplifications. However, they were able to clarify some detailed structures, such as the waves in the macroscopic quantities traveling in the column and an oscillatory motion in the atmosphere during eclipse, that had not been noticed in Ref. [5]. Indeed, it is a formidable task to find such detailed structures of the atmospheric behavior by the DSMC simulation, especially in the case of unsteady problems. Therefore, we may emphasize that the present results provide a deeper understanding of the phenomena found in Ref. [5] and thus complement this reference.

References

[1] A. P. Ingersoll, M. E. Summers, and S. G. Schlipf, *Icarus* **64**, 375–390 (1985).

[2] J. V. Austin and D. B. Goldstein, *Icarus* **148**, 370–383 (2000).

[3] W. H. Smyth and M. C. Wong, *Icarus* **171**, 171–182 (2004).

[4] A. C. Walker, S. L. Gratiy, D. B. Goldstein, C. H. Moore, P. L. Varghese, L. M. Trafton, D. A. Levin, and B. Stewart, *Icarus* **207**, 409–432 (2010).

[5] C. H. Moore, D. B. Goldstein, P. L. Varghese, L. M. Trafton, and B. Stewart, *Icarus* **201**, 585–597 (2009).

[6] G. A. Bird, *Phys. Fluids* **6**, 1518–1519 (1963).

[7] G. A. Bird, *Molecular Gas Dynamics and the Direct Simulation of Gas Flows,* Oxford University Press, Oxford (1994).

[8] S. Kosuge, K. Aoki, T. Inoue, D. B. Goldstein, and P. L. Varghese, *Icarus* **221**, 658–669 (2012).

[9] S. Kosuge and K. Aoki, *Rarefied Gas Dynamics, AIP Conf. Proc.*, **1501**, 1541–1548 (2012).

[10] P. Andries, K. Aoki, and B. Perthame, *J. Stat. Phys.* **106**, 993–1018 (2002).

[11] Y. Sone, *Molecular Gas Dynamics: Theory, Techniques, and Applications,* Birkhäuser, Boston (2007).

[12] K. Aoki, Y. Sone, and T. Yamada, *Phys. Fluids A* **2**, 1867–1878 (1990).

[13] T. Ohwada, Y. Sone, and K. Aoki, *Phys. Fluids A* **1**, 1588–1599 (1989).

[14] F. Xiao, T. Yabe, G. Nizam, and T. Ito, *Comput. Phys. Commun.* **94**, 103–118 (1996).

[15] H. Takewaki, A. Nishiguchi, and T. Yabe, *J. Comput. Phys.* **61**, 261–268 (1985).

Department of Mechanical Engineering and Science
Kyoto University
Kyoto 615-8540
JAPAN
E-mail address: kosuge.shingo.6r@kyoto-u.ac.jp

京都大学・工学研究科・機械理工学専攻　小菅　真吾